Oscillating bound states in non-Markovian photonic lattices

Kian Hwee Lim [1,*,†] Wai-Keong Mok [1,2,*,‡] and Leong-Chuan Kwek [1,3,4,5]

[1] *Centre for Quantum Technologies, National University of Singapore, 3 Science Drive 2, Singapore 117543*

[2] *California Institute of Technology, Pasadena, California 91125, USA*

[3] *MajuLab, CNRS-UNS-NUS-NTU International Joint Research Unit, UMI 3654, Singapore*

[4] *National Institute of Education, Nanyang Technological University, 1 Nanyang Walk, Singapore 637616*

[5] *School of Electrical and Electronic Engineering Block S2.1, 50 Nanyang Avenue, Singapore 639798*

(Received 11 November 2022; accepted 6 February 2023; published 17 February 2023)

It is known that the superposition of two bound states in the continuum (BICs) leads to the phenomenon of an oscillating bound state, where excitations mediated by the continuum modes oscillate persistently. We perform exact calculations for the oscillating BICs in a one-dimensional photonic lattice coupled to a "giant atom" at multiple points. Our work is significantly distinct from previous proposals of oscillating BICs in continuous waveguide systems due to the presence of a finite energy band contributing band-edge effects. In particular, we show that the bound states outside the energy band are detrimental to the oscillating BIC phenomenon, and can be suppressed by increasing either the number of coupling points or the separation between each coupling point. Crucially, non-Markovianity is necessary for the existence of oscillating BICs, and the oscillation amplitude increases with the characteristic delay time of the giant atom interactions. We also propose an initialization scheme in the BIC subspace. Our work be experimentally implemented on current photonic waveguide array platforms and opens up prospects in utilizing reservoir engineering for the storage of quantum information in photonic lattices.

DOI: 10.1103/PhysRevA.107.023716

I. INTRODUCTION

The study of interactions between atoms and photons traces its history all the way back to the inception of quantum mechanics itself. Since then, we have acquired a better understanding of atom-photon interactions which underpins the foundation of many quantum technologies such as atomic clocks [1] and trapped-ion quantum computers and simulators [2–4], which harness the interaction of atoms with lasers. In many studies of atom-photon interactions, one often makes the dipole approximation [5], which assumes that the size of the atom is much smaller than the wavelength of the light. This is especially valid in optical regimes where the length scale of the atom ($\sim 10^{-10}$ m) is orders of magnitude smaller than the wavelength of light ($\sim 10^{-7}$ m). Under the dipole approximation, the time taken for the light to pass through a single atom is neglected, thus simplifying the interaction model. In the field of waveguide quantum electrodynamics (QED) [6,7], which studies the interactions of atoms with a continuum of bosonic modes in a waveguide, the dipole approximation corresponds to modeling the atoms as coupled to individual points along the waveguide [8,9]. These atoms could either be actual atoms [10] or artificial atoms such as quantum dots [11–13] and superconducting qubits [14–16]. A more complete overview of works done in this vein can be found in Refs. [17–19].

However, this paradigm of dipole approximation in waveguide QED was recently broken with the discovery of the so-called "giant atoms" [20,21], by coupling each atom to two or more points on the waveguide. This was originally achieved by coupling the superconducting artificial atom (working in the microwave regime) to surface acoustic waves (SAW). Due to the low SAW velocity, for a given frequency the wavelength of sound is no longer assumed to be large compared to the size of the superconducting artificial atom. An alternative method to engineer giant atom coupling is by meandering the transmission line such that the atom interacts with the waveguide at multiple locations [22,23]. In these setups, we can no longer ignore the phase acquired by the light propagating in the one-dimensional (1D) waveguide during the interaction with the giant atoms. Remarkably, by tuning the acquired phase [20], one obtains fascinating phenomena such as prolonged coherence time of a giant atom [20,23], decoherence-free interactions between two giant atoms [22,23], and the non-exponential decay of a giant atom [24,25], which have also been experimentally demonstrated in recent years.

Another novel feature of giant atoms in waveguide QED is the existence of oscillating bound states in the continuum (BICs), which is a genuine non-Markovian effect due to the significant time delay for information to propagate between the various coupling points of a giant atom [24]. The non-Markovianity manifests as a persistent oscillation of energy in the waveguide trapped between the coupling points of a giant atom, which behaves akin to a cavity. This is in stark contrast

*These authors contributed equally to this work.

†kianhwee_lim@u.nus.edu

‡darielmok@caltech.edu

to the irreversible loss of energy from the giant atom to the waveguide in the Markovian regime. Thus, these oscillating BICs can potentially be harnessed to preserve quantum information in a non-Markovian bath by stabilizing the photonic quantum state, which we will show in this paper.

In the continuous waveguide case, it is usual to linearize the dispersion relation about the atom's energy, since the coupling to the waveguide is weak [7]. The waveguide can then be regarded as having a linear dispersion with an infinite bandwidth. Instead of using a continuous waveguide such as a transmission line, we consider a 1D photonic lattice which acts as the reservoir for the giant atom. The key difference between the 1D photonic lattice that we consider here and the continuous waveguide proposed in Ref. [26] is the presence of a finite energy band where the band edge becomes significant, which restricts the allowed BICs. Experimentally, this can be achieved using a photonic waveguide array where each waveguide is side-coupled to others via the evanescent field produced by the photon propagating inside the waveguides [27,28]. This has been proposed to simulate the nonexponential decay of a photonic giant atom [29] which is simultaneously coupled to multiple lattice sites. We also note that while oscillating BICs have been reported in a discrete lattice system with two giant atoms [30], manifesting as an effective Rabi oscillation between the atoms, our work requires only a single giant atom to produce oscillating BICs.

As we will see, having a finite band gives rise to new conditions for the oscillating BIC phenomenon, which are distinct from those derived for the continuous waveguide. Moreover, we now need to consider the effect of bound states outside the energy band. These bound states outside the energy band are out of the continuum of allowed propagating modes and will henceforth be called bound states outside the continuum (BOCs). As will be explained in more detail later, these BOCs are detrimental to quantum information storage, as they are states with an exponentially decaying wave function around the coupling points of the giant atom to the 1D photonic lattice. Hence, even though it is possible to observe oscillatory behavior in the emitter excitation probability with BOCs [31], we distinguish the oscillating BICs which we study here, which allow for perfect quantum information storage, from oscillations induced by BOCs, which do not. We also show that the oscillating BIC is a consequence of the time-delayed interactions mediated by the 1D photonic lattice, and that a longer time delay generally results in a higher amplitude for the BIC, which reduces the information leakage. A longer time delay also suppresses the unwanted contributions from the BOCs which hinder the ability of the GA to store and retrieve quantum information. This allows us to find the optimal conditions for oscillating BICs.

This paper is organized as follows: Firstly, we introduce the model Hamiltonian and the theory behind BICs in Sec. II. Our main theoretical results are presented in Sec. III, where we derive the conditions for oscillating BICs in our system as well as optimal conditions to minimize the detrimental impact of BOCs. Thereafter, we present some numerical results in Sec. IV which support our analytical calculations. To demonstrate the feasibility of our theoretical results, we propose an experimental implementation of our work achievable on state-of-the art photonic hardware in Sec. V. Finally, we conclude in Sec. VI and provide several directions for future research.

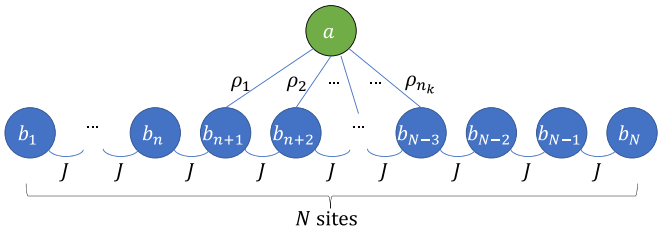

FIG. 1. An illustration of the Hamiltonian in Eq. (1). Here, we have N lattice sites arranged in a chain with bosonic annihilation operator b_n for each lattice site. The N lattice sites are described by a tight-binding Hamiltonian $H_{\rm wg}$ with coupling strength J. We also have an extra lattice site described by the annihilation operator a with Hamiltonian H_a, which we shall call the "giant atom" lattice site, due to its multiple coupling points to the 1D photonic lattice. The giant atom lattice site is coupled to the lattice sites $n_1, n_2, \ldots, n_k$ with coupling strengths $\rho_1, \rho_2, \ldots, \rho_{n_k}$, respectively. This coupling is described by the Hamiltonian $H_{\rm int}$.

II. THEORY

A. Model Hamiltonian

The Hamiltonian for the combined atom-lattice system can be written as $H = H_a + H_{\rm wg} + H_{\rm int}$, given in Eq. (1) as (setting $\hbar = 1$)

$$H_a = \omega_a a^\dagger a + U a^{\dagger 2} a^2 \tag{1a}$$

$$H_{\rm wg} = J \sum_{n=1}^{N-1} (b_n^\dagger b_{n+1} + \text{H.c.}) \tag{1b}$$

$$H_{\rm int} = \sum_{j=1}^{M} \rho_j (a^\dagger b_{n_j} + \text{H.c.}), \tag{1c}$$

where a is the annihilation operator for the giant atom satisfying the bosonic commutation relation $[a, a^\dagger] = 1$, and b_n are the annihilation operators for the 1D photonic lattice with $[b_n, b_m^\dagger] = \delta_{mn}$. ω_a is the detuning between the giant atom and the photonic lattice. The N lattice sites are coupled to each other via a tight-binding Hamiltonian with interaction strength J. The giant atom is coupled to M arbitrary lattice sites $\{n_1, \ldots, n_M\}$ with strength ρ_j, $j = 1, \ldots, M$. Here, N is chosen to be a large number such that we can treat the lattice as an infinite 1D chain in both the left and right directions. The giant atom has an anharmonicity U, which we will take $U \to \infty$ such that it is equivalent to treating the giant atom as a two-level system. An illustration can be found in Fig. 1. As is shown in Appendix A, the Hamiltonian described by Eq. (1) can also be written in k space in the first Brillouin zone as

$$H_a = \omega_a a^\dagger a \tag{2a}$$

$$H_{\rm wg} = \int_{-\pi}^{\pi} dk\, \omega(k) c^\dagger(k) c(k) \tag{2b}$$

$$H_{\rm int} = \int_{-\pi}^{\pi} dk \{G(k) a^\dagger c(k) + \text{H.c.}\} \tag{2c}$$

by defining the k-space annihilation operators $c(k)$ through the discrete Fourier transform

$$c(k) = \frac{1}{\sqrt{2\pi}} \sum_{n=1}^{N} b_n e^{-ikn}, \quad b_n = \frac{1}{\sqrt{2\pi}} \int_{-\pi}^{\pi} e^{ikn} c(k)\, dk. \tag{3}$$

The operators for the lattice $c(k)$ obey the bosonic commutation relations $[c(k), c^\dagger(k')] = \delta(k - k')$ with the dispersion relation $\omega(k) = 2J\cos(k)$ and the spectral coupling function $G(k) = \frac{1}{\sqrt{2\pi}} \sum_{j=1}^{M} \rho_j e^{ikn_j}$. In general, $G(k)$ depends on the specific geometry of our system, such as the number of coupling points M between the giant atom and the 1D photonic lattice and also the locations of the coupling points $n_1, n_2, \ldots, n_M$. In previous works [24,26], the dispersion relation is linearized and the energy band formed by the waveguide modes is approximated to be infinite such that the band-edge effects become negligible. As we will see later, by confining the allowed energies to be in $[-2J, 2J]$, we obtain new conditions for oscillating BICs. Before that, it is helpful to first review the essential physics of BIC in this system.

B. Bound states in the continuum

A system is said to have a BIC if there is an energy eigenstate with energy Ω, where Ω lies in the band of allowed energies of the system. BICs are theoretically very interesting because conventionally, we would not expect a bound state to exist within a continuum of propagating states that would carry the energy of the bound state away, and yet these BICs truly exist and have been investigated both theoretically and experimentally [32–35]. Specifically, for the setup that we are considering, the system has a BIC with energy Ω if $\Omega \in [-2J, 2J]$, which is defined by the tight-binding dispersion relation $\omega(k) = 2J\cos(k)$. Furthermore, for a BIC at energy Ω to exist, either the density of modes vanishes at $\omega = \Omega$ so that there is no mode in the continuum for the bound state to decay into, or the coupling to the continuum vanishes at $\omega = \Omega$. Lastly, since the BIC is a bound state by definition, we also require the energy eigenstate at frequency Ω to have a finite norm. The above conditions can be stated in more mathematically precise terms [35].

Defining the density of modes $\rho(\omega) \equiv \frac{\partial k}{\partial \omega}$, the density of modes vanishing at $\omega = \Omega$ means that we require $\frac{\partial k}{\partial \omega}|_\Omega = 0$, which is not possible for the tight-binding dispersion relation. Thus, by designing the giant atom coupling, we enforce the condition for the coupling to the continuum to vanish at Ω

$$|G[k(\Omega)]|^2 = 0. \tag{4}$$

If we restrict ourselves to the one-excitation subspace, a general time-dependent state of the system can be written as

$$|\psi(t)\rangle = \psi_a(t)|1_a\rangle + \int_{-\pi}^{\pi} dk\, \psi(k,t)|1_k\rangle, \tag{5}$$

where $|1_a\rangle = a^\dagger|0\rangle$, $|1_k\rangle = c^\dagger(k)|0\rangle$. By considering an energy eigenstate $|E\rangle$ also in the one-excitation subspace, we obtain

$$\Omega - \omega_a = \int_{-\pi}^{\pi} dk \frac{|G(k)|^2}{\Omega - \omega(k)} \tag{6}$$

by comparing the coefficients of $|1_a\rangle$ and $|1_k\rangle$ in the energy eigenvalue equation $H|E\rangle = \Omega|E\rangle$. Hence, the requirement that we have an energy eigenstate with energy Ω within the band implies that the solution of Eq. (6) for Ω lies in the range $[-2J, 2J]$. The preceding calculation also gives us an expression for the coefficient of $|1_k\rangle$, from which we can deduce that the finite norm requirement of the energy eigenstate is equivalent to $\rho(\omega)|G[k(\omega)]|^2$ vanishing in the limit $\omega \to \Omega$ at least as fast as $\sim(\Omega - \omega)^2$. The integral in Eq. (6) can be evaluated by first evaluating the self-energy $\Sigma(s)$ defined by

$$\Sigma(s) = \int_{-\pi}^{\pi} dk\, \frac{|G(k)|^2}{is - \omega(k)}, \tag{7}$$

from which we get

$$\Omega - \omega_a = \mathrm{Re}[\Sigma(s = -i\Omega \pm 0^+)]. \tag{8}$$

A detailed derivation of the above equations is presented in Appendix B.

C. Decay dynamics

In order to probe the decay dynamics of the giant atom into the 1D photonic lattice, we initialize the system with one excitation in the giant atom and the lattice in the vacuum state. Mathematically, with reference to Eq. (5), we have $\psi_a(0) = 1$ and $\psi(k, 0) = 0\, \forall k \in [-\pi, \pi]$. From the Schrödinger equation $i\partial_t|\psi(t)\rangle = H|\psi(t)\rangle$ with these initial conditions, it can be shown (see Appendix C) that $\Sigma(s)$ controls the time-dependent probability amplitude $\psi_a(t)$ through the equation

$$\psi_a(t) = \sum_{\text{All residues}} \frac{ie^{st}}{is - \omega_a - \Sigma(s)}. \tag{9}$$

From Eq. (9), we see that poles on the right-hand side of the equation with a nonzero real component will lead to a decay in $\psi_a(t)$. On the other hand, for the poles on the right-hand side of the equation that lie on the imaginary axis, i.e., if $s = -i\Omega$, the exponential factor in the numerator will be $e^{-i\Omega t}$, which is nondecaying and physically represents a BIC arising from the giant atom decay. We note that (see Appendix B) when there exists an Ω that fulfills Eq. (8) as well as $|G[k(\Omega)]|^2 = 0$, then Ω will be a pole on the imaginary axis, which means that we will have a BIC at the frequency Ω.

These BICs arising from giant atom decay are very interesting because by construction they are immune to decay into the 1D lattice, and hence can be used in a manner analogous to the so-called "dark states" for purposes like storing quantum information, etc. [36,37]. Denoting the BIC energies as Ω_j, which satisfy both Eq. (8) and Eq. (4), with simple poles at $s = -i\Omega_j$, we have

$$\begin{aligned}\psi_a(t) &= \sum_j \lim_{s \to -i\Omega_j} \left[\frac{ie^{st}}{is - \omega_a - \Sigma(s)} (s + i\Omega) \right] \\ &= \sum_j \frac{e^{-i\Omega_j t}}{1 + i\Sigma'(-i\Omega_j)},\end{aligned} \tag{10}$$

where we used L'Hopital's rule and also defined $\Sigma' = \partial_s \Sigma$ to get to the second line. Moreover, by noting that

$$\psi_a(t) = \sum_E e^{-iEt} |\langle 1_a|E\rangle|^2, \tag{11}$$

we obtain the emitter contribution of each BIC as

$$\left|\phi_a^{(j)}\right|^2 \equiv |\langle 1_a|\Omega_j\rangle|^2 = \frac{1}{1+i\Sigma'(-i\Omega_j)}. \tag{12}$$

The usefulness of each of these BICs can be quantified by the magnitude of $|\phi_a^{(j)}|^2$, since a large $|\phi_a^{(j)}|^2$ implies that the giant atom has a high probability of being excited despite the existence of decay channels in the continuum for it to decay into.

III. OSCILLATING BOUND STATES

Consider the case of giant atom decay in the one-excitation subspace again. From Eq. (9), if there exist two BICs at frequency Ω_α and Ω_β that have relatively large residues compared to the other BICs, we have $\psi_a(t) \approx Ae^{-i\Omega_\alpha t} + Be^{-i\Omega_\beta t}$ for some complex numbers A and B. This means that the emitter probability $|\psi_a(t)|^2$ oscillates sinusoidally with frequency $|\Omega_\alpha - \Omega_\beta|/2\pi$. We can also infer the same fact by looking at Eq. (11). In this scenario, we say that our system exhibits an oscillating BIC. Interestingly, we will show that these oscillating BICs inherently require non-Markovianity in the system, resulting in a bath-induced stabilization of a single-photon quantum state which can be used both as a photon trapped in a cavity as well as a storage for quantum information. Ideally, we would want $|A| = |B|$ so that at some time t, we have $|\psi_a(t)|^2 = 0$, which means that by turning off the giant atom couplings to the 1D lattice chain at that time, we can release the stored photon into the 1D chain.

Let us now calculate the conditions in which the setup shown in Fig. 1 exhibits an oscillating BIC. Consider the case where the giant atom has M coupling points equally spaced apart by n_0 sites on the photonic lattice. For N lattice sites, let the giant atom be coupled to sites $0, n_0, 2n_0, \ldots, (M-1)n_0$ with a uniform coupling strength ρ_0. For this particular setup, we have

$$G(k) = \frac{\rho_0}{\sqrt{2\pi}} \sum_{j=0}^{M-1} e^{ijkn_0}. \tag{13}$$

As shown in Appendix E, it is not possible for an oscillating BIC to exist when $M = 2$, consistent with the results in a continuous linear waveguide [26]. Hence, we consider the case when $M \geqslant 3$ for which oscillating BICs exist. Detailed calculations can be found in Appendix D. We will summarize some of the key results here. We first calculate $|G(k)|^2$ to be

$$|G(k)|^2 = \frac{\rho_0^2}{2\pi}\left[M + 2\sum_{r=1}^{M-1}(M-r)\cos(kn_0 r)\right], \tag{14}$$

which means that when we enforce Eq. (4) for the coupling to the continuum to vanish, we have

$$k = \frac{2\pi}{n_0}\left(m \pm \frac{1}{M}\right), \tag{15}$$

where $m \in \mathbb{Z}$. Furthermore, Eq. (7) and Eq. (14) together give us

$$\Sigma(s) = \frac{\mp i\rho_0^2}{\sqrt{s^2+4J^2}}\left[M + 2\sum_{r=1}^{M-1}(M-r)\alpha^{rn0}\right] \tag{16}$$

$$\alpha = \left(\frac{\mp i\sqrt{s^2+4J^2} + is}{2J}\right), \tag{17}$$

where we have the negative sign in both α and $\Sigma(s)$ above when $\mathrm{Re}(s) > 0$ and the positive sign when $\mathrm{Re}(s) < 0$. Since the subsequent results are the same regardless of whether we consider $\mathrm{Re}(s) > 0$ or $\mathrm{Re}(s) < 0$, we will restrict ourselves to the $\mathrm{Re}(s) > 0$ case. Thereafter, from Eq. (8), Eq. (16), and Eq. (17) we have

$$\Omega - \omega_a = \frac{-i\rho_0^2}{\sqrt{4J^2-\Omega^2}}\left[M + 2\sum_{r=1}^{M-1}(M-r)(e^{in_0\theta})^r\right], \tag{18}$$

where $\theta = \arctan(-\sqrt{4J^2-\Omega^2}/\Omega)$. Hence, to obtain an oscillating BIC, we need to solve Eq. (18) together with Eq. (15) to obtain two eigenenergies Ω_1 and Ω_2 such that the coupling to the continuum vanishes at these two energies.

At this juncture, we consider the case where $\omega_a = 0$, such that the giant atom energy is positioned at the band center. This is done so that the BIC energies Ω_1, Ω_2 are symmetric about the band center, i.e., $\Omega_1 = -\Omega_2$, which is necessary to obtain perfectly sinusoidal oscillations of the giant atom emitter probability. From Eq. (15), we see that n_0 being an odd number will not give us BIC energies that are symmetric about the band center. Hence, n_0 is restricted to be an even number, which give us two possibilities, $n_0 = 2(2l)$ or $n_0 = 2(2l+1)$, where $l \in \mathbb{Z}^+$. Since the giant atom energy is positioned at the band center, we would expect the BIC energies that are closer to the band center to correspond to states that have a larger emitter probability. Using that criteria, we find that the optimal condition for oscillating BIC occurs for the $n_0 = 4l$ case (see Appendix D), from which we get the BIC energies $\pm\Omega_{\mathrm{BIC}}$ given by

$$\Omega_{\mathrm{BIC}} = 2J\sin\left(\frac{2\pi}{Mn_0}\right). \tag{19}$$

We can then obtain the corresponding ρ_0 for $\pm\Omega_{\mathrm{BIC}}$ by substituting Eq. (19) into Eq. (18) together with $\omega_a = 0$ to obtain

$$\left(\frac{\rho_0}{J}\right)^2 = \frac{2}{M}\tan\left(\frac{\pi}{M}\right)\sin\left(\frac{4\pi}{Mn_0}\right), \tag{20}$$

resulting in an oscillating BIC at the frequency $\Omega_{\mathrm{BIC}}/\pi$. Now we can obtain the emitter probabilities of each BIC by substituting Eq. (19) and Eq. (20) into Eq. (12) to obtain

$$\left|\phi_a^{(\mathrm{BIC})}\right|^2 \equiv \langle 1_a| \pm \Omega_{\mathrm{BIC}}\rangle|^2 = \frac{ie^{-\frac{4i\pi}{M}}\left(1+e^{\frac{2i\pi}{M}}\right)\left[-1+\left(ie^{\frac{2i\pi}{Mn_0}}\right)^{n_0}\right]^3 \csc^2\left(\frac{\pi}{M}\right)\cos^2\left(\frac{2\pi}{Mn_0}\right)}{4\left[2n_0\sin\left(\frac{4\pi}{Mn_0}\right)+\sin\left(\frac{2\pi(n_0-2)}{Mn_0}\right)+\sin\left(\frac{2\pi(n_0+2)}{Mn_0}\right)\right]}. \tag{21}$$

From the emitter probabilities obtained above, using Eq. (9) and Eq. (10), we see that in the long time limit after all the non-BIC states have propagated away from the giant atom to the left and right ends of the lattice chain, we would expect oscillations in the emitter probability of the giant atom with amplitude $(2|\phi_a^{(\mathrm{BIC})}|^2)^2$. From Eq. (21), we note that for all values of $n_0 = 4l$, $l \in \mathbb{Z}^+$, $|\phi_a^{(\mathrm{BIC})}|^2$ increases monotonically with M, eventually saturating at the limiting value $|\phi_a^{(\mathrm{BIC})}|^2 = 1/3$. Consequently, for any value of n_0, having a larger number of coupling points M leads to higher-amplitude oscillating BICs. It is also helpful to use Eq. (21) to compute the asymptotic behavior of $|\phi_a^{(\mathrm{BIC})}|^2$ as $n_0 \to \infty$, which we can write as

$$\left|\phi_a^{(\mathrm{BIC})}\right|^2 = \frac{1}{1+\frac{4\pi}{M}\csc\left(\frac{2\pi}{M}\right)} + \frac{A}{n_0^2} + O\left(\frac{1}{n_0^4}\right),$$
$$\text{where } A = \frac{4\pi^2 \sin\left(\frac{2\pi}{M}\right)\left[3M\sin\left(\frac{2\pi}{M}\right) - 4\pi\right]}{3M\left[M\sin\left(\frac{2\pi}{M}\right) + 4\pi\right]^2}. \tag{22}$$

By defining $\tau = (Mn_0)/v_g$ as the time taken for the photon to propagate between the first coupling point and the Mth coupling point (i.e., the size of the giant atom), where $v_g = 2J$ is the group velocity at the band center, and $\Gamma^{-1} = (M^2\rho_0^2/J)^{-1}$ as the characteristic timescale for the giant atom decay, we can quantify the amount of non-Markovianity in our system through the quantity τ/Γ^{-1}, which can be written as

$$\frac{\tau}{\Gamma^{-1}} = M^2 n_0 \sin\left(\frac{4\pi}{Mn_0}\right)\tan\left(\frac{\pi}{M}\right) \tag{23}$$
$$= 4M\pi\tan\left(\frac{\pi}{M}\right) - \frac{32\left[\pi^3\tan\left(\frac{\pi}{M}\right)\right]}{3M}\frac{1}{n_0^2} + O\left(\frac{1}{n_0^4}\right), \tag{24}$$

where to get from the first line to the second line, we computed the asymptotic behavior as $n_0 \to \infty$. From Eq. (24), we see that at large n_0 the non-Markovianity in our system, which has the same $1/n_0^2$ scaling as the expressions for the BIC emitter probabilities in Eq. (22). This allows us to conclude that a stronger non-Markovianity in our system arising from the time delay for information to propagate between the giant atom coupling points results in better oscillating BICs, though the amount of non-Markovianity quantified by τ/Γ^{-1} eventually reaches a plateau. The presence of the plateau means that even though τ increases as n_0 increases, which leads to a greater non-Markovianity in the system, this effect is quickly balanced by an increase in the giant atom lifetime Γ^{-1}, which is a result of a decreased coupling strength ρ_0. In practice, n_0 should of course not be too large, since the oscillation period scales as $\sim n_0$, which might lead to more decoherence. Fortunately, the fast convergence $O(1/n_0^2)$ of the emitter probabilities means that a moderate n_0 is already sufficient to observe good oscillating BICs.

Finally, we note that for all values of $n_0 = 4l$, $l \in \mathbb{Z}^+$, as $M \to \infty$, τ/Γ^{-1} monotonically decreases to a limiting value of $4\pi^2$. This implies that our system with an oscillating BIC is inherently non-Markovian in nature, since there is a nonnegligible lower bound to τ/Γ^{-1}.

A. Role of imperfections: Bound states outside the continuum

BOCs are energy eigenstates of the Hamiltonian that have energy out of the range $[-2J, 2J]$. For these states, the wave number k is complex [38], which means that these states are unable to propagate in the 1D lattice chain and hence they have a significant probability amplitude in $|1_a\rangle$, with an exponentially decaying wave function around the coupling points of the giant atom. These states are imperfections to our oscillating BIC for two reasons. Firstly, for an oscillating BIC produced by giant atom decay, we want the emitter probability to be high for the two BICs involved at $\pm\Omega_{\mathrm{BIC}}$, and low for all the other energy eigenstates. Yet these BOCs have a large atomic component and hence they act as imperfections to our sinusoidal oscillation as per Eq. (9). Secondly, these states leak energy outside the giant-atom coupling points due to the exponential decay of the photon amplitude from the coupling points.

To characterize the effect of BOCs on oscillating BICs produced by giant atom decay, we first use Eq. (20) to obtain ρ_0 corresponding to the oscillating BIC condition. Then, we solve for the BOC energies Ω_{BOC}, where $|\Omega_{\mathrm{BOC}}| > 2J$ in Eq. (6) with $\omega_a = 0$. In the limit of $n_0 \to \infty$, the two BOC energies can be found as

$$\Omega_{\mathrm{BOC}} \approx \pm 2J\left(1 + \frac{2\pi^2\tan(\pi/M)^2}{M^2 n_0^2}\right), \tag{25}$$

with the emitter probability

$$\left|\phi_a^{(\mathrm{BOC})}\right|^2 \sim \frac{4\pi^2\tan(\pi/M)^2}{M^2}\frac{1}{n_0^2}. \tag{26}$$

This means that for a given value of M, at large n_0, the contributions from the BOCs to the oscillations are suppressed by a factor of $1/n_0^2$. By comparing Eq. (26) and Eq. (24), we see that a larger non-Markovianity in our system characterized by a larger τ/Γ^{-1} leads to reduced imperfections from the BOC. We also note that having a larger number of coupling points M leads to a diminished effect of the BOCs on our oscillating bound states, which can be explained by how a larger value of M leads to a smaller coupling ρ_0 between the giant atom and the lattice chain.

B. Initialization in the BIC subspace

Up till now, we have considered the case of giant atom decay into the 1D lattice chain. If instead we are given the ability to initialize the state of the lattice sites in the chain, which is possible for some experimental platforms such as a side-coupled waveguide array through pulse shaping techniques, we can eliminate the effects of the BOCs even at low n_0 and also obtain perfect storage of quantum information within the legs of the giant atom. This is especially important for small values of M like $M = 3$, since from Eq. (26) we see that the emitter probability of the BOC states increases as M decreases. Hence, we shall temporarily restrict ourselves to $M = 3$ here, though it should be clear that the method below generalizes for any positive integer values of M.

We first write the states corresponding to the BICs at $\pm\Omega_{\mathrm{BIC}}$ as

$$|\pm\rangle = \phi_{a,\pm}|1_a\rangle + \sum_n \phi_{n,\pm}|n\rangle. \tag{27}$$

Without loss of generality, we can set $\phi_{a,\pm} = |\phi_a^{(\mathrm{BIC})}|$ since eigenstates are defined up to a global phase. Here $\phi_{n,\pm}$ are

the photon amplitudes in real space, which for $M = 3$ we can calculate $\phi_{n,\pm}$ to be given by

$$\phi_{n,+} = C \times \begin{cases} (-1)^n \exp\left(i\frac{2\pi n}{3n_0}\right) \\ -\exp\left(-i\frac{2\pi n}{3n_0}\right), 0 \leqslant n \leqslant n_0 \\ (-1)^{n+1} \exp\left[i\frac{2\pi}{3}\left(\frac{n}{n_0} - 2\right)\right] \\ +\exp\left[-i\frac{2\pi}{3}\left(\frac{n}{n_0} - 2\right)\right], n_0 \leqslant n \leqslant 2n_0 \\ 0, \quad \text{else} \end{cases}, \tag{28}$$

where

$$C = \frac{-i^{n+1}\phi_a\rho_0}{2J\cos\left(\frac{2\pi}{3n_0}\right)} \tag{29}$$

and $\phi_{n,-} = (-1)^{n+1}\phi^*_{n,+}$. The above calculation also means that the state

$$|p\rangle \equiv \frac{1}{\sqrt{2}}(|+\rangle - |-\rangle) = \frac{1}{\sqrt{2}}\sum_n (\phi_{n,+} - \phi_{n,-})|n\rangle \tag{30}$$

is a state with no probability amplitude in $|1_a\rangle$ and with photon amplitudes in real space only within the M coupling points of the giant atom. Thus, if we initialize the state in $|p\rangle$, then there will be zero excitation leakage outside of the giant atom and

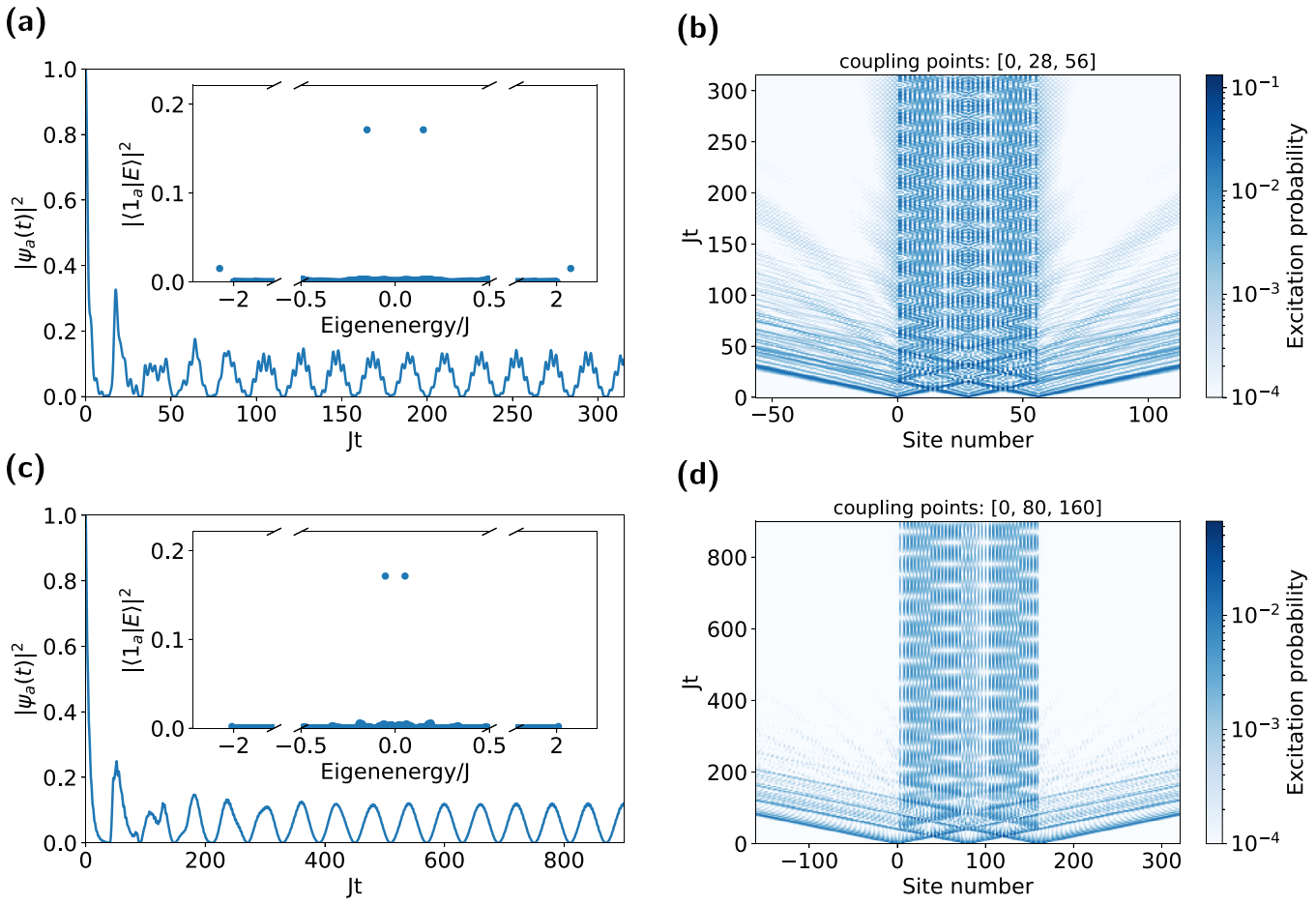

FIG. 2. Simulation results for giant atom decay into the 1D photonic lattice for the case of $M = 3$ coupling points. The coupling strength ρ_0 between the giant atom and the 1D photonic lattice can be calculated from Eq. (20). (a and c) Excitation probability against time for the giant atom lattice site for $n_0 = 28$ and $n_0 = 80$, respectively. In the insets, we plot the emitter probability for each of the eigenstates of H. As can be seen in the insets, there are two eigenstates with energies in the continuum $[-2J, 2J]$ that are symmetrical about 0 and have a emitter probability. (b and d) Excitation probability against time for some of the lattice sites in the 1D photonic lattice for $n_0 = 28$ and $n_0 = 80$, respectively. Initially we see some transient behavior as the nonbound states decay into the 1D lattice chain and are propagated away to the left and right ends of the 1D photonic lattice. Thereafter, we see the photon being trapped in between the $M = 3$ coupling points with nonzero probability and oscillating between these three points with time. By comparing (a) and (c), we see that the $n_0 = 28$ case has oscillations that are not perfectly sinusoidal, due to the effect of the relatively large BOC emitter probabilities, as can be seen in the inset of (a). As was previously explained and is seen here in (b), the presence of these BOCs with large emitter probabilities for the $n_0 = 28$ case also lead to a leakage of the photon excitation probability beyond the coupling points of the giant atom. We can also see that this imperfection is absent for the $n_0 = 80$ case.

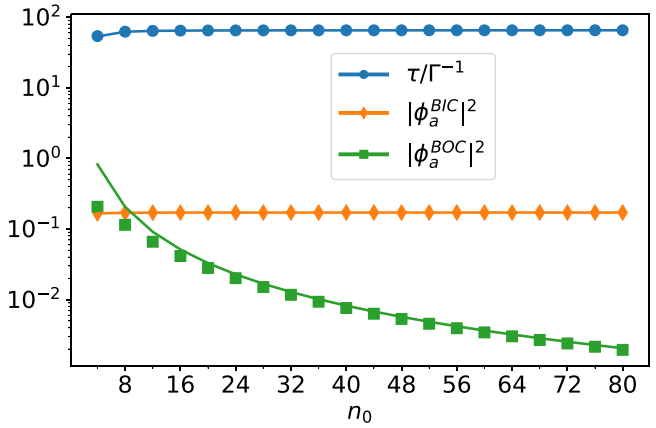

FIG. 3. A plot showing how the emitter probabilities for the BICs, given by $|\phi_a^{(\mathrm{BIC})}|^2$, and the BOCs, given by $|\phi_a^{(\mathrm{BOC})}|^2$, scale as the number of sites n_0 between each coupling point increases. On this figure we show the values computed numerically (scatter plot) as well as the values computed from our asymptotic expansions (continuous lines) as $n_0 \to \infty$ for the case where there are $M = 3$ coupling points between the giant atom and the 1D lattice chain. On the same figure we also plot how τ/Γ^{-1} scales with n_0. As can be seen, as τ/Γ^{-1} increases and saturates at a value given by Eq. (24), $|\phi_a^{(\mathrm{BIC})}|^2$ also increases and saturates at a value given by Eq. (22). On the other hand, $|\phi_a^{(\mathrm{BOC})}|^2$ decreases monotonically with increasing n_0. We see that clearly, as the amount of non-Markovianity τ/Γ^{-1} in our system increases, we get better oscillating bound states.

the lattice sites within the M coupling points. Furthermore, since the states $|\pm\rangle$ are orthogonal to the BOCs, the imperfections in the oscillations due to the BOCs are eliminated by construction. Lastly, we note that for $M = 3$ the photon amplitudes are real and only differ in phase by 0 or π, which makes it more feasible for practical implementation.

IV. NUMERICAL RESULTS

Here we first present in Fig. 2 some results for the $M = 3$ giant atom decay coupled to a 1D photonic lattice with various values of n_0. For $M = 3$, starting with a single excitation in the giant atom, in the absence of imperfections due to the BOCs, we should expect sinusoidal oscillations in the excitation probability of the giant atom lattice site with oscillation amplitude $(2|\phi_a^{(\mathrm{BIC})}|^2)^2 \approx 0.117411$, where we have used Eq. (22) to obtain $|\phi_a^{(\mathrm{BIC})}|^2 \approx 0.171$ for $M = 3$. However, for the $M = 3$ case, as is seen in Fig. 3, the BOC emitter probabilities are actually quite substantial, especially at small values of n_0. Hence, this leads us to consider a strategy for the $M = 3$ case where instead of considering giant atom decay, we initialize the lattice sites in the initial state Eq. (30) to eliminate the effects of the BOCs, resulting in complete storage of quantum information within the legs of the giant atoms and perfectly sinusoidal oscillations in the excitation probability of the giant atom lattice site with oscillation amplitude $2|\phi_a^{(\mathrm{BIC})}|^2 \approx 0.33$. An example for the $n_0 = 4$ case is shown in Fig. 4. The amplitude and phase of the initial photon excitation at each of the lattice sites can be found using Eq. (30), where examples for various values of n_0 are shown in Fig. 5. Finally, to show the effect of increasing M on the quality of the giant atom oscillating BIC, we plot the case of giant atom decay for the $M = 50$ and $n_0 = 4$ case in Fig. 6. We note that for this value of M, we should expect the excitation probability in the giant atom lattice site to oscillate with an amplitude of $(2|\phi_a^{(\mathrm{BIC})}|^2)^2 \approx 4/9$ as $|\phi_a^{(\mathrm{BIC})}|^2$ approaches the asymptotic value of $1/3$ for increasing values of M.

V. EXPERIMENTAL IMPLEMENTATION

The Hamiltonian in Eq. (1) can be simulated on a variety of platforms, such as coupled cavity arrays [39,40] and photonic waveguide arrays [41–45]. In the case of a photonic waveguide array, we would have one photonic waveguide, which we call the giant atom waveguide, coupled to M different photonic waveguides that are already coupled to each other to form a linear chain of N waveguides, where the coupling is due to the evanescent field produced by the photon propagating within the waveguide. As the photon propagates in the waveguide, we have the relation $z = ct$, where c is the group velocity of the photon in the waveguide and z is the distance along the waveguide that the photon has propagated for.

Following our formalism above, the nearest-neighbor coupling of the photonic waveguides in the linear chain with coupling strength J gives us the tight binding Hamiltonian H_{wg}, whereas the coupling between the giant atom waveguide and the linear chain of waveguides at M different points, each spaced n_0 apart, with coupling strength ρ_0 gives us the interaction Hamiltonian H_{int}. Taking the constraints of current experimental capabilities in mind, we propose an experimental setup for the case where $M = 3$ and $n_0 = 4$ using the BIC subspace initialization in Fig. 7. For this photonic waveguide array system, the BIC initialization according to Fig. 7 can be achieved deterministically with a spatial light modulator that modulates a single photon source [47]. Alternatively, one can also prepare the oscillating BIC probabilistically by initializing an excitation only in the giant atom waveguide and perform photodetection on the sites outside of the giant atom coupling points, and postselect on the no-detection events.

In Fig. 7 we have also denoted the next-nearest-neighbor coupling between the giant atom waveguide and the sites 0 ± 1, $n_0 \pm 1$, and $2n_0 \pm 1$ with ρ_1, and also the next-nearest-neighbor hopping between the lattice sites 0 ± 1, $n_0 \pm 1$, and $2n_0 \pm 1$ with J'. In general, the presence of J' and ρ_1 are unwanted imperfections, yet we note that by choosing the geometry and the distances accordingly as per the inset in Fig. 7, we can minimize the contributions from ρ_1 as well as J'. To do so, we first use Eq. (19) to calculate the emitter energies for $n_0 = 4$, which would give us the oscillation period $T = \pi$ for the oscillating BIC. This means that to see an appreciable number of oscillations, we could simulate up to $Jz = 5T \approx 15$. Now, suppose that experimentally, we can only have photonic waveguides with length z_{max}. This means that we require $J = 5T/z_{\mathrm{max}}$. Henceforth, we shall assume $z_{\mathrm{max}} = 100$ mm, which has been done experimentally before [48]. From Eq. (20), we obtain $\rho_0/J = 1$, which tells us to set $\rho_0 = J$. It is known that the evanescent coupling strength between waveguides decays exponentially with the distance between them [46]. Using the experimental values obtained in Ref. [46] for the aforementioned exponential relationship

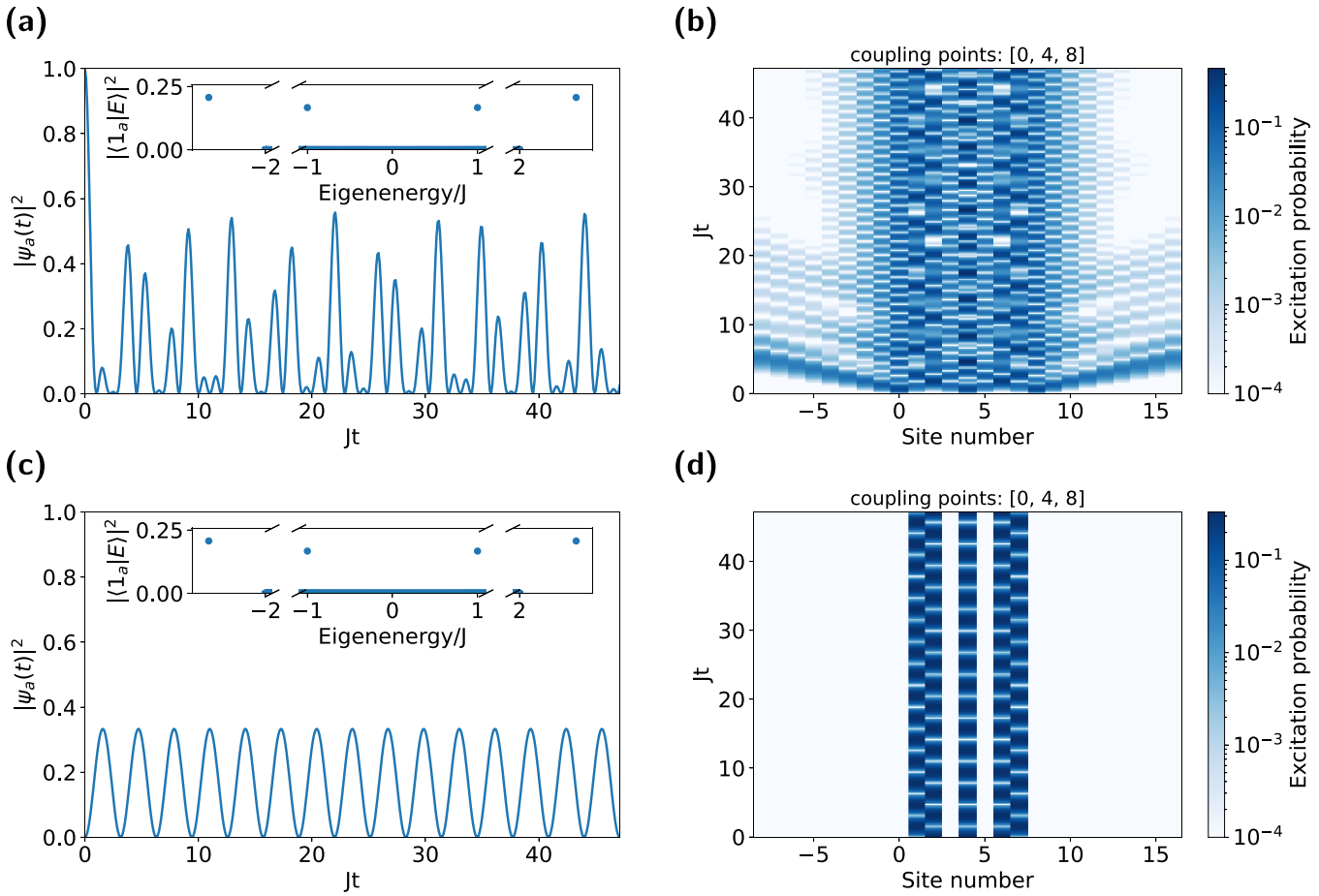

FIG. 4. Similar to Fig. 2, in (a) and (b) we consider the case of giant atom decay into the 1D lattice chain but with $M = 3$ coupling points and $n_0 = 4$ sites between each coupling point. In (c) and (d), we also consider the case where we have $M = 3$ coupling points and $n_0 = 4$ sites but with the giant atom lattice site initially in the vacuum state and the 1D lattice chain initialized in the state $|p\rangle$ according to Eq. (30). Remarkably, using Eq. (20), the required giant atom coupling strength is $\rho_0/J = 1$. Due to the presence of the two BOCs with large emitter probabilities, for the case of the giant atom decay in (a) and (b), we see that the oscillation of the giant atom excitation probability in (a) is highly nonsinusoidal. Moreover, in (b), we see that there is a leakage of photon excitation probability beyond the coupling points due to the presence of the BOC, which is nonideal. In (c) and (d), we see that because we are starting in the BIC subspace, the contributions due to the BOCs are totally eliminated. We see perfectly sinusoidal oscillations of the giant atom excitation probability in (c), and we also see that the photon excitation probability is strictly confined to within the coupling points of the giant atom to the 1D lattice.

between coupling strength and distance, together with the geometry of the proposed setup in the inset of Fig. 7, we obtain $\rho_0 = J = 0.15\,\mathrm{mm}^{-1}$, $\rho_1 = 0.0286\rho_0$, and $J' = 0.0286J$, which is nearly negligible. Thus, our proposed oscillating BICs are experimentally feasible using state-of-the-art photonic waveguide arrays.

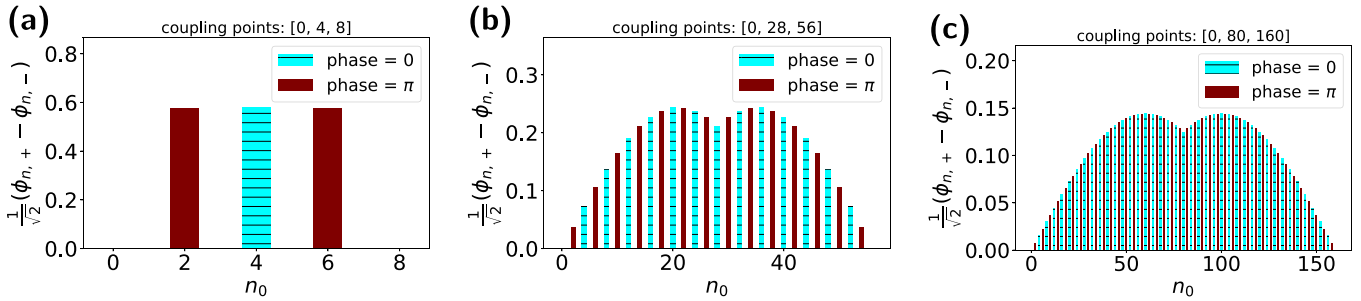

FIG. 5. Here we show the amplitudes and the phases of the photonic excitation required to initialize the 1D lattice chain in the state $|p\rangle$ given by Eq. (30) for the case of $M = 3$ coupling points between the giant atom and the 1D lattice chain. In (a)–(c), we plot the cases where we have $n_0 = 4$, $n_0 = 28$, and $n_0 = 80$, respectively. Sites with a phase of 0 are indicated by a blue (lighter) color with a striped line within, whereas sites with a phase of π are indicated by a solid red (darker) color.

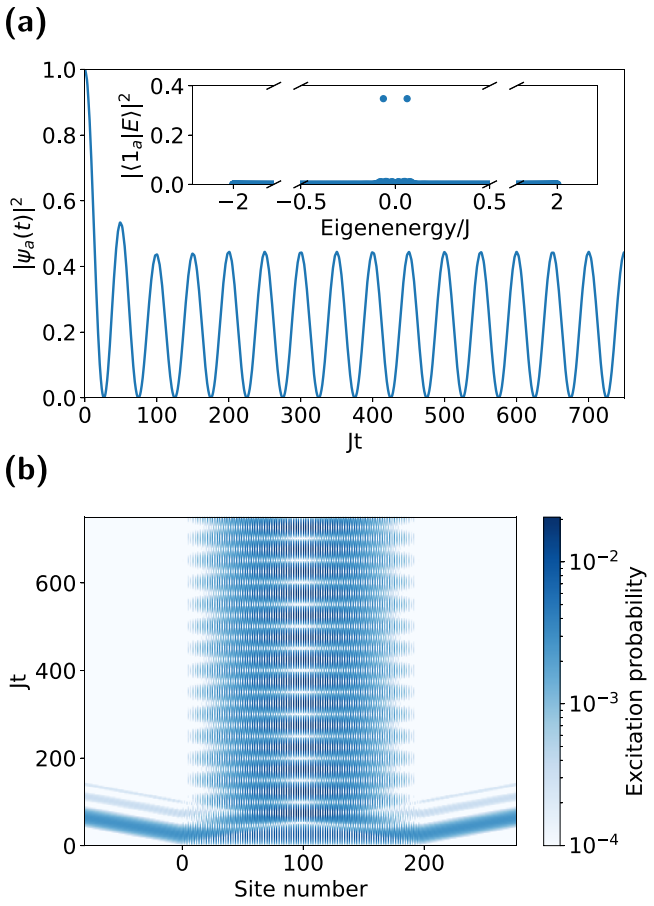

FIG. 6. The analog of Fig. 2 except that we have $M = 50$ coupling points between the giant atom and the 1D photonic lattice for $n_0 = 4$. As can be seen from the inset of (a), the emitter probabilities from the BOC are heavily suppressed as per Eq. (26), which leads to perfectly sinusoidal oscillations of the excitation probability of the giant atom lattice site. We also see in (b) that the negligible BOC emitter probability leads to an absence of loss of photonic excitation probability into the 1D lattice chain. By comparing (a) in this figure to Fig. 2, we see that a larger value of M leads to larger amplitude oscillations in the excitation probability of the giant atom lattice site even for a comparatively small value of n_0, as per Eq. (21).

Simulation results for $M = 3$ and $n_0 = 4$ when $\rho_1 = 0$ and $J' = 0$ can be found in Fig. 4. The corresponding results when $\rho_1 = 0.0286\rho_0$ and $J' = 0.0286J$ can be found in Fig. 8.

VI. CONCLUSION

In this paper, we study the phenomenon of oscillating BIC in a discrete 1D photonic lattice using a single emitter coupled to multiple lattice sites, which can be considered as the discrete analog of a giant atom coupled to a continuous waveguide. The key difference between our work and the oscillating BICs found in continuous waveguide systems [26] is the presence of a finite energy band, which contributes band-edge effects to the giant atom dynamics. This gives us new conditions for the existence of oscillating BICs which lead to persistent oscillations of energy between the coupling points of the giant atom to the 1D lattice. The presence of

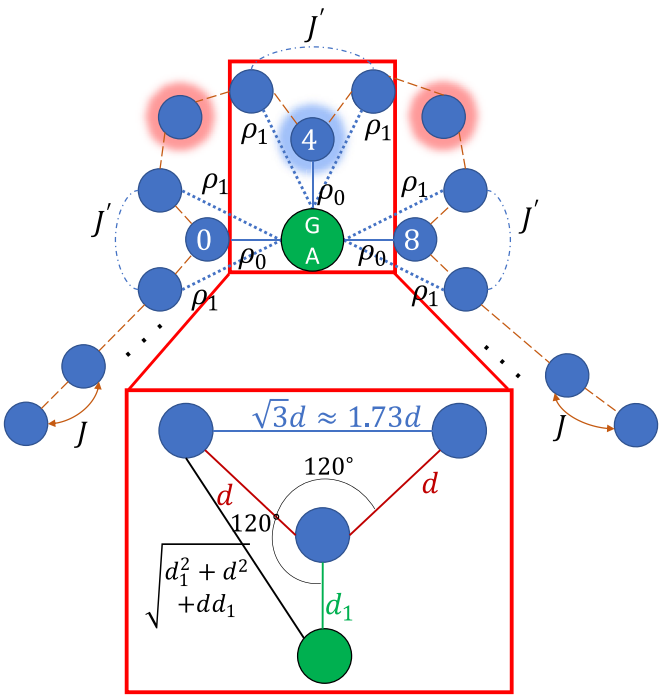

FIG. 7. Possible experimental setup to see oscillating BICs. Here, we have $M = 3$ and $n_0 = 4$. The giant atom waveguide is in green, with the letters "GA" inside, whereas the waveguides in the waveguide chain are in blue. The coupling strength ρ_0 can be found from Eq. (20). Here, ρ_1 is the coupling between the giant atom and the next-nearest-neighbor sites and J' is the hopping strength between the sites that are ± 1 from the coupling point. In this setup, we start with the giant atom in the vacuum state and instead initialize the rest of the waveguide chain in the state $|p\rangle$ according to Eq. (30). This means that as per Fig. 5 for the case where $n_0 = 4$, we need to send in a photon with equal probability amplitude in waveguides 2, 4, and 6, which we have highlighted. The red glow (sites 2 and 6) indicates a phase of π for the photon, whereas a waveguide with a blue glow (site 4) indicates a phase of 0. For the array of photonic waveguides, the coupling strength between each waveguide decays exponentially with the distance between the waveguides [46], hence by choosing the distances d, d_1 in the experimental setup appropriately as per the inset, we can obtain $\rho_1 \ll \rho_0$ and $J' \ll J$, which allows us to neglect the next-nearest-neighbor interactions.

BOCs hinders the trapping of excitation between the giant atom coupling points and is detrimental to the sinusoidal oscillations in the giant atom probability. Crucially, we find that these unwanted BOCs can be suppressed drastically by increasing either the number of coupling points M or the number of lattice sites n_0 between each coupling point, with the BOC contribution scaling as $1/M^2$ and $1/n_0^2$. With this, we can summarize our key results for the conditions to produce optimal oscillating BICs to be (1) $n_0 = 4l, l \in \mathbb{Z}^+$ sites between each coupling point, (2) large n_0, and (3) large M. In practice, however, we find that a moderate M and n_0 suffice to achieve good oscillating BICs with significant giant atom probability. Alternatively, by initializing the lattice sites in the BIC subspace which we have calculated, the BOC contributions can be completely eliminated, resulting in perfect oscillating BICs even for small M and n_0. We stress that the oscillating BIC in our system is inherently a non-

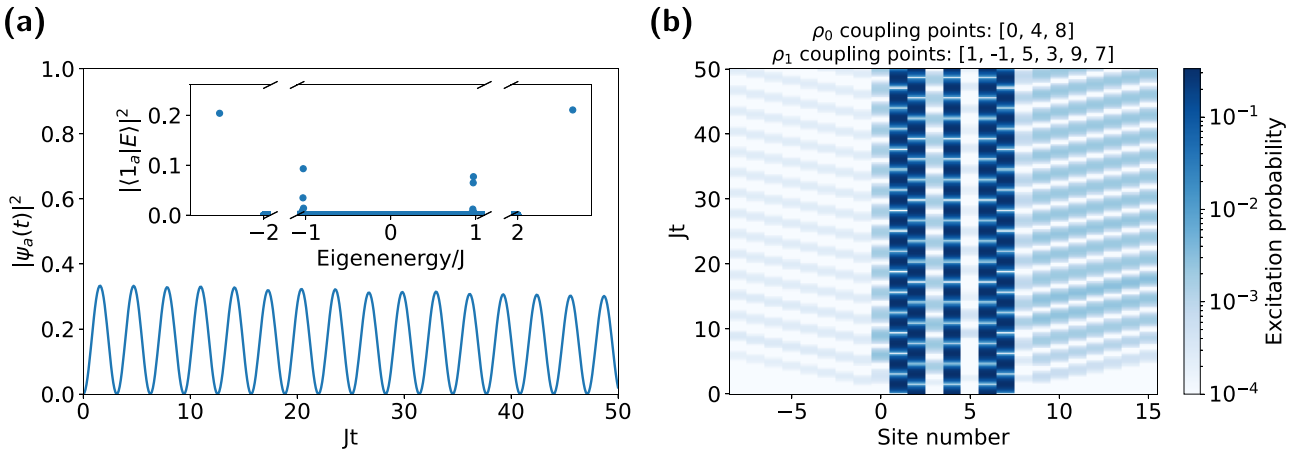

FIG. 8. Simulation results for the proposed experimental implementation with the setup in Fig. 7. Here, we initialize the waveguide array in the state $|p\rangle$ and with the giant atom lattice site in the vacuum state. Also, with reference to Fig. 7, we consider the case where we have $\rho_1 = 0.0286\rho_0$ and $J' = 0.0286J$ to show the impact of these experimental imperfections on our simulation. The corresponding ideal case for which $\rho_1 = J' = 0$ can be found in Figs. 4(c) and 4(d). By comparing the ideal case with (a) and (b) in this figure, we see that the presence of experimental imperfections leads to a leakage of photon excitation probability beyond the coupling points of the giant atom, yet the effect is nearly negligible up to $Jz = 15$, which is a large enough value of Jz to see an appreciable number of oscillations.

Markovian phenomenon due to the significant propagation time between the giant atom coupling points compared to the relaxation timescale of the giant atom. Moreover, we show that as the non-Markovianity in our system increases, the oscillation amplitude of the BICs increases, improving the storage of quantum information within the coupling points. To illustrate the feasibility of our theoretical model, we propose an experimental implementation of our system on photonic waveguide arrays and show that our oscillating BICs can be practically achieved even with current experimental limitations.

Our work provides a firm theoretical basis for oscillating BICs in discrete systems. In particular, oscillating BICs in discrete systems offer new possibilities that cannot be replicated in continuous systems, such as the ability to initialize the system in the BIC subspace by simply controlling the amplitude and phase of the excitation at particular lattice sites. This allows us to achieve long-time storage of quantum information within the confines of the giant atom coupling points, limited only by the intrinsic coherence time of the photonic lattice. Our setup can also be regarded as an effective cavity, serving as a physical implementation of non-Markovian cavity-QED setups [49–53]. While we have considered the tight-binding dispersion relation in this work, the phenomenon of oscillating BICs can be generally observed in discrete systems with other dispersion relations, which can be considered for future work. Another promising direction is to study the oscillating BIC phenomenon in higher-dimensional lattices [54] or in synthetic dimensions [55,56].

ACKNOWLEDGMENTS

K.H.L, W.K.M., and L.C.K. are grateful to the National Research Foundation, Singapore and the Ministry of Education, Singapore for financial support. The authors thank Anton Frisk Kockum for useful discussions.

APPENDIX A: WRITING EQ. (1) IN k SPACE

From Eq. (3), we can express $H_{\rm wg}$ as

$$
\begin{aligned}
H_{\rm wg} &= J\sum_n b_n^\dagger b_{n+1} + \text{H.c.} \\
&= \frac{J}{2\pi}\iint dk\,dk' \sum_n e^{i(k'-k)n} e^{ik'} c^\dagger(k)c(k') \\
&\quad + \frac{J}{2\pi}\iint dk\,dk' \sum_n e^{-i(k'-k)n} e^{-ik'} c^\dagger(k')c(k) \\
&= \frac{J}{2\pi}\iint dk\,dk' \sum_n e^{i(k'-k)n} e^{ik'} c^\dagger(k)c(k') \\
&\quad + \frac{J}{2\pi}\iint dk'\,dk \sum_n e^{-i(k-k')n} e^{-ik} c^\dagger(k)c(k') \\
&= J\iint dk\,dk' \left(\frac{1}{2\pi}\sum_n e^{i(k'-k)n}\right)(e^{ik'} + e^{-ik})c^\dagger(k)c(k') \\
&= J\iint dk\,dk' \delta(k'-k)(e^{ik'} + e^{-ik})c^\dagger(k)c(k') \\
&= J\int dk\,(e^{ik} + e^{-ik})c^\dagger(k)c(k) \\
&= \int dk\, 2J\cos(k)c^\dagger(k)c(k) \\
&= \int dk\,\omega(k)c^\dagger(k)c(k), \qquad \text{(A1)}
\end{aligned}
$$

where we have defined $\omega(k) \equiv 2J\cos(k)$. Here, we have used the fact that for $(k'-k) \in [0, 2\pi)$, $\frac{1}{2\pi}\sum_n e^{i(k'-k)n} = \delta(k'-k)$. Similarly, we can also express $H_{\rm int}$ as

$$
\begin{aligned}
H_{\rm int} &= \sum_{j=1}^{k} \rho_j (a^\dagger b_{n_j} + \text{H.c.}) \\
&= \sum_{j=1}^{k} \rho_j \left\{ a^\dagger \left[\frac{1}{\sqrt{2\pi}} \int_{-\pi}^{\pi} dk\, e^{ikn_j} c(k) \right] + \text{H.c.} \right\}
\end{aligned}
$$

$$= \int_{-\pi}^{\pi} dk \left\{ \left(\frac{1}{\sqrt{2\pi}} \sum_{j=1}^{k} \rho_j e^{ikn_j} \right) a^\dagger c(k) + \text{H.c.} \right\}$$
$$\equiv \int_{-\pi}^{\pi} dk \, \{G(k) a^\dagger c(k) + \text{H.c.}\}, \tag{A2}$$

where we have defined $G(k) = (\frac{1}{\sqrt{2\pi}} \sum_{j=1}^{K} \rho_j e^{ikn_j})$.

APPENDIX B: DERIVATION OF CONDITIONS FOR BIC

First, to derive Eq. (6) and the condition for the BIC to have a finite norm, we shall first write our energy eigenstate in the one-excitation subspace as

$$|E\rangle = \phi_a |1_a\rangle + \int dk \, e(k) |1_k\rangle, \tag{B1}$$

where $\phi_a = \langle 1_a | E \rangle$ and $e(k) = \langle 1_k | E \rangle$. Thereafter, we consider the energy eigenvalue equation $H|E\rangle = \Omega |E\rangle$. To evaluate $H|E\rangle$, we use the commutation relations $[a, a^\dagger] = 1$ and $[c(k), c^\dagger(k')] = \delta(k - k')$, and finally we arrive at

$$H|E\rangle = \left[\omega_a \phi_a + \int dk \, G(k) e(k) \right] |1_a\rangle + \int dk \, [\omega(k) e(k) + G^*(k) \phi_a] |1_k\rangle. \tag{B2}$$

Comparing the above equation with $\Omega |E\rangle = \Omega [\phi_a |1_a\rangle + \int dk \, e(k) |1_k\rangle]$, we arrive at two simultaneous equations:

$$\Omega \phi_a = \omega_a \phi_a + \int dk \, G(k) e(k) \tag{B3a}$$
$$\Omega e(k) = \omega(k) e(k) + G^*(k) \phi_a, \tag{B3b}$$

which we can then solve to obtain Eq. (6). Next, we note that in the one-excitation subspace, we have

$$\langle E | E \rangle = |\phi_a|^2 + \int dk \, |e(k)|^2$$
$$= |\phi_a|^2 \left(1 + \int dk \, \frac{|G(k)|^2}{[\Omega - \omega(k)]^2} \right)$$
$$= |\phi_a|^2 \left(1 + \int d\omega \, \frac{\rho(\omega) |G[k(\omega)]|^2}{(\Omega - \omega)^2} \right), \tag{B4}$$

where in the second line, we used Eq. (B3b) and in the third line, we used $\rho(\omega) \equiv \frac{\partial k}{\partial \omega}$. Hence, we see that the requirement that $|E\rangle$ has a finite norm corresponds to $\rho(\omega)|G[k(\omega)]|^2$ vanishing at least as fast as $\sim(\Omega - \omega)^2$ as $\omega \to \Omega$.

Next, to derive Eq. (8), we note that

$$\Sigma(s = -i\Omega \pm 0^+) = \int_{-\pi}^{\pi} dk \frac{|G(k)|^2}{\Omega - \omega(k)}$$
$$= \int_{-2J}^{2J} d\omega \frac{\rho(\omega) |G[k(\omega)]|^2}{\Omega - \omega}$$
$$= \lim_{\epsilon \to 0} \left(\int_{-2J}^{\Omega - \epsilon} d\omega \, \frac{\rho(\omega) |G[k(\omega)]|^2}{\Omega - \omega} + \int_{\Omega + \epsilon}^{2J} d\omega \, \frac{\rho(\omega) |G[k(\omega)]|^2}{\Omega - \omega} \right)$$
$$+ \int_C d\omega \, \frac{\rho(\omega) |G[k(\omega)]|^2}{\Omega - \omega}$$
$$= \mathcal{P} \left(\int_{-2J}^{2J} d\omega \frac{\rho(\omega) |G[k(\omega)]|^2}{\Omega - \omega} \right) \mp i\pi \rho(\Omega) |G[k(\Omega)]|^2, \tag{B5}$$

where in the second last line, we note that the contour C is a semicircular contour either in the top half or bottom half of the complex plane, depending on the sign of $\pm 0^+$, and in the last line we used the residue theorem for the special case of a semicircular contour. $\mathcal{P}()$ here denotes the Cauchy principal value of the integral enclosed in parentheses. Taking the real part of the last line, Eq. (8) follows immediately. We note here that if Ω also fulfills Eq. (4), then the second term vanishes, which gives us

$$\Sigma(s = -i\Omega \pm 0^+) = \text{Re}[\Sigma(s = -i\Omega \pm 0^+)]. \tag{B6}$$

APPENDIX C: DECAY DYNAMICS

Here, we derive Eq. (9). By writing down the Schrodinger equation $H|\psi(t)\rangle = i \frac{\partial}{\partial t} |\psi(t)\rangle$ in the one-excitation subspace as per Eq. (5), we arrive at two coupled equations:

$$i \frac{\partial \psi_a(t)}{\partial t} = \omega_a \psi_a(t) + \int_{-\pi}^{\pi} G(k) \psi(k, t) dk \tag{C1a}$$
$$i \frac{\partial \psi(k, t)}{\partial t} = \omega(k) \psi(k, t) + G^*(k) \psi_a(t). \tag{C1b}$$

To solve the two above equations for $\psi_a(t)$, we follow the standard procedure of first integrating the "bath" equation, which is Eq. (C1b) in our case, to get

$$\psi(k, t) = -iG^*(k) e^{-i\omega(k)t} \int_0^t dt' e^{i\omega(k)t'} \psi_a(t') + e^{-i\omega(k)t} \psi(k, 0). \tag{C2}$$

Then, we substitute the above equation into Eq. (C1a) to get

$$\frac{\partial \psi_a(t)}{\partial t} = -i\omega_a \psi_a(t) - \int_{-\pi}^{\pi} dk \, |G(k)|^2 e^{-i\omega(k)t} \times \int_0^t dt' \, e^{i\omega(k)t'} \psi_a(t') - iA(t), \tag{C3}$$

where $A(t) \equiv \int_{-\pi}^{\pi} dk \, G(k) e^{-i\omega(k)t} \psi(k, 0)$. Next, we take the Laplace transform on both sides of the above equation by defining $\tilde{\psi}_a(s) = \int_0^\infty dt \, e^{-st} \psi_a(t)$. By also using the fact that $\int_0^\infty dt \, e^{-st} \frac{\partial \psi_a(t)}{\partial t} = s\tilde{\psi}_a(s) - \psi_a(0)$, and defining $\tilde{A}(s)$ as the Laplace transform of $A(t)$, we arrive at

$$s\tilde{\psi}_a(s) - \psi_a(0) = -i\omega_a \tilde{\psi}_a(s) - i\tilde{A}(s) - \int_{-\pi}^{\pi} dk \, |G(k)|^2 \int_0^\infty dt \, e^{-[s + i\omega(k)]t} F(t), \tag{C4}$$

where $F(t) \equiv \int_0^t dt' e^{i\omega(k)t'} \psi_a(t')$. Realizing that $\frac{d}{dt} F(t) = e^{i\omega(k)t} \psi_a(t)$, we perform integration by parts on $\int_0^\infty dt \, e^{-(s + i\omega(k))t} F(t)$ and after some algebra finally arrive at

$$[s + i\omega_a + i\Sigma(s)] \tilde{\psi}_a(s) = -i\tilde{A}(s) + \psi_a(0), \tag{C5}$$

where $\Sigma(s)$ as defined in Eq. (7). By inserting into the above equation the initial conditions corresponding to the case of giant atom decay, $\psi_a(0) = 1$ and $\psi(k, 0) = 0$ for all k, we finally arrive at

$$\tilde{\psi}_a(s) = \frac{1}{s + i\omega_a + i\Sigma(s)}, \tag{C6}$$

which we can invert via the Bromwich integral to give us $\psi_a(t)$ in the following manner,

$$\begin{aligned}\psi_a(t) &= \frac{1}{2\pi i}\int_{\lambda-i\infty}^{\lambda+i\infty} \frac{e^{st}}{s + i\omega_a + i\Sigma(s)} \\ &= \sum_{\text{All residues}} \frac{e^{st}}{s + i\omega_a + i\Sigma(s)},\end{aligned}$$

where to go from the first line to the second line, we pick λ sufficiently large so that all the poles of the integrand lie on the left of the line $\lambda + it$, $t \in (-\infty, \infty)$. The second line is Eq. (9) in the main text. We note that in going from the first line to the second line, we have ignored the contributions from the integration over any paths induced by possible branch cuts. This is because we will mainly use the above equation to study the behavior of BICs, which are poles on the imaginary axis and hence lead to long-term, nondecaying behavior of $\psi_a(t)$. The integration over any paths induced by possible branch cuts leads to transient decay behavior which we are not interested in.

APPENDIX D: DETAILED CALCULATIONS FOR SECTION III IN THE MAIN TEXT

1. Derivation of Eq. (16)

First of all, we note the important integral result

$$\begin{aligned}I_n(s) &= \int_{-\pi}^{\pi} dk\, \frac{e^{ikn}}{is - \cos(k)} \\ &= \frac{-2\pi i}{\sqrt{s^2+1}}(is \mp i\sqrt{s^2+1})^{|n|}\end{aligned} \tag{D1}$$

where we have the minus sign when $\text{Re}(s) > 0$ and the positive sign when $\text{Re}(s) < 0$. The result can be derived by making the substitution $z = e^{ik}$ and thereafter computing the resultant complex integral

$$\begin{aligned}I_n(s) &= \oint_C dz\, \frac{z^n}{is - (1/2)(z + z^{-1})}\frac{1}{iz} \\ &= 2i\oint_C dz\, \frac{z^n}{z^2 - 2isz + 1} \\ &= 2i\oint_C dz\, \frac{z^n}{(z - z_1)(z - z_2)},\end{aligned} \tag{D2}$$

where the contour C is the unit circle in the complex plane and $z_1 = i(s + \sqrt{s^2+1})$, $z_2 = i(s - \sqrt{s^2+1})$. The above integral can then be easily evaluated by the Cauchy residue theorem. Now, we can show that $\text{Re}(s) > 0$ implies that $|z_1| > 1$, $|z_2| < 1$, which means that z_2 is a simple pole in C. On the other hand, $\text{Re}(s) < 0$ implies that $|z_1| < 1$, $|z_2| > 1$, which means that z_1 is a simple pole in C. Moreover, if $n < 0$, then we also have an nth order pole at $z = 0$ in C. Putting all of these together with the fact that $z_1 z_2 = 1$, which means that $z_1^{-|n|} = z_2^{|n|}$, we can arrive at Eq. (D1) after some algebra.

Thereafter, using the above result we can easily derive the following integral, with n being a nonnegative integer:

$$\int_{-\pi}^{\pi} dk \frac{\cos(nk)}{is - 2J\cos(k)} = \frac{-2\pi i}{\sqrt{s^2+4J^2}}\left(\frac{is \mp i\sqrt{s^2+4J^2}}{2J}\right)^n, \tag{D3}$$

where again we have the minus sign when $\text{Re}(s) > 0$ and the positive sign when $\text{Re}(s) < 0$. Next, we can derive

$$\begin{aligned}|G(k)|^2 &= \frac{\rho^2}{2\pi}\sum_{j=0}^{M-1}\sum_{l=0}^{M-1} e^{ikn_0(j-l)} \\ &= \frac{\rho^2}{2\pi}\left[M + 2\sum_{r=1}^{M-1}(M - r)\cos(kn_0 r)\right],\end{aligned} \tag{D4}$$

where in going from the first line to the next, we realize that there are M terms of $e^{ik(0)n_0}$, $(M-1)$ terms of $e^{ik(1)n_0}$ and its complex conjugate, $(M-2)$ terms of $e^{ik(2)n_0}$ and its complex conjugate, and so on, until at last we have 1 term of $e^{ik(M-1)n_0}$ and its complex conjugate. With the form of $|G(k)|^2$ above and Eq. (D3), we can get Eq. (16) from Eq. (7).

2. Derivation of oscillating BIC conditions

Since we are working with $\omega_a = 0$, we want to look for two BICs as near the band center as possible with energies $\pm\Omega_{\text{BIC}}$, where Ω_{BIC} is a positive value to be determined. Hence, we want to minimize the quantity

$$\left|\frac{\Omega}{2J}\right| = \cos\left[\frac{2\pi}{n_0}\left(m \pm \frac{1}{M}\right)\right] \tag{D5}$$

over all integer values of m. Note that in the above expression, we have already substituted Eq. (15) into the dispersion relation $\omega(k) = 2J\cos(k)$. One way to perform this minimization is to first solve m in the equation $|\Omega/2J| = 0$ and then round the value of m to the closest integer. When we solve $|\Omega/2J| = 0$, we obtain two cases:

$$\frac{2\pi}{n_0}\left(m \pm \frac{1}{m}\right) = \frac{\pi}{2} \Rightarrow m = \frac{n_0}{4} \mp \frac{1}{m} \tag{D6a}$$

$$\frac{2\pi}{n_0}\left(m \pm \frac{1}{m}\right) = \frac{3\pi}{2} \Rightarrow m = \frac{3n_0}{4} \mp \frac{1}{m}. \tag{D6b}$$

At this juncture, before we round the value of m obtained above to the closest integer, we note that there are two cases we need to consider: either $n_0 = 2(2l)$ or $n_0 = 2(2l+1)$ where $l \in \mathbb{Z}$. In the former case where $n_0 = 4l$, the closest integer value of m would be $m = n_0/4$ or $m = 3n_0/4$, which would give us the BIC frequencies in Eq. (19) when we substitute those values of m into Eq. (D5). Thereafter, we can obtain ρ_0 by substituting those frequencies into Eq. (18) to obtain Eq. (20).

In the latter case where $n_0 = 4l + 2$, the closest integer values of m would be $m = n_0/4 \pm 1/2$ or $m = 3n_0/4 \pm 1/2$, corresponding to two possible BIC frequencies,

$$\Omega_{\text{BIC}} = \sin\left[\frac{\pi}{n_0}\left(1 \pm \frac{2}{M}\right)\right].$$

However, when we substitute $\Omega_{\rm BIC} = \sin[(\pi/n_0)(1-2/M)]$ into Eq. (18), for the case of $\omega_a = 0$, we end up with $\rho_0^2 < 0$, which means that we are only left with $\Omega_{\rm BIC} = \sin[(\pi/n_0)(1+2/M)]$ for the $n_0 = 4l+2$ case. However, since this is further from the band center as compared to the $n_0 = 4l$ case, the resultant bound states would have lower emitter probability. Hence, we can conclude that $n_0 = 4l$ would give optimal oscillating BICs.

As an example, for the case where $M = 3$ and $n_0 = 4l+2$, $n_0 > 2$, we have the BIC frequency $|\Omega| = 2J\sin(\frac{5\pi}{3n_0})$, which gives us

$$\rho_0^2 = \frac{2J^2}{\sqrt{3}}\sin\left(\frac{10\pi}{3n_0}\right). \tag{D7}$$

Using Eq. (12), we find that the emitter probability

$$\left|\phi_a^{\rm BIC}\right|^2 \to \frac{9}{9+20\sqrt{3}\pi} \approx 0.0764 \tag{D8}$$

as $n_0 \to \infty$, which is considerably smaller than the optimal value ≈0.171 when n_0 is an integer multiple of 4 for $M = 3$.

3. Derivation of Eq. (25) and Eq. (26)

To derive Eq. (25), the method is to solve Eq. (16) using both Eq. (17) and Eq. (8) for the case where $\omega_a = 0$ and $|\Omega| > 2J$. The $|\Omega| > 2J$ condition is because we are trying to solve for Ω outside the energy band. We note that there are two cases for us to consider, namely, $\mathrm{Re}(s) > 0$, corresponding to $s = -i\Omega + 0^+$ and $\mathrm{Re}(s) < 0$, corresponding to $s = -i\Omega - 0^+$. As we will see, the $\mathrm{Re}(s) > 0$ case gives us the BOC energy for $\Omega < -2J$, and the $\mathrm{Re}(s) < 0$ case gives use the BOC energy for $\Omega > 2J$. First, we consider the $\mathrm{Re}(s) > 0$ case. In this case, we have the equation

$$\left(\frac{\Omega}{2J}\right)^2 = -\frac{1}{4}\left(\frac{\rho_0}{J}\right)^2 \frac{1}{\sqrt{\left(\frac{\Omega}{2J}\right)^2 - 1}}\left\{M + 2\sum_{r=1}^{M-1}(M-r)\left[\frac{\Omega}{2J} + \sqrt{\left(\frac{\Omega}{2J}\right)^2 - 1}\right]^{n_0 r}\right\}, \tag{D9}$$

where we have used $\sqrt{4J^2 - \Omega^2} = i\sqrt{\Omega^2 - 4J^2}$, since $|\Omega| > 2J$. Now, we substitute $\Omega' = \Omega/2J$ as well as Eq. (20) for ρ_0/J to get

$$\Omega'\sqrt{\Omega'^2 - 1} = -\frac{1}{4}\frac{2}{M}\tan\left(\frac{\pi}{M}\right)\sin\left(\frac{4\pi}{Mn_0}\right)\left[M + 2\sum_{r=1}^{M-1}(M-r)(\Omega' + \sqrt{\Omega'^2 - 1})^{n_0 r}\right], \tag{D10}$$

In the $n_0 \to \infty$ limit, for the above equation to have a solution, we must have $\Omega' + \sqrt{\Omega'^2 - 1} < 1$, which means $\Omega < -2J$. Hence, taking the $n_0 \to \infty$ limit, we have

$$\Omega'\sqrt{\Omega'^2 - 1} = -\frac{2}{M}\tan\left(\frac{\pi}{M}\right)\left(\frac{\pi}{Mn_0}\right)M. \tag{D11}$$

Solving for Ω' in the above equation subject to the condition that $\Omega < -2J$, we have

$$\Omega' = -\sqrt{\frac{1}{2}\sqrt{\frac{16\pi^2\tan^2\left(\frac{\pi}{M}\right)}{M^2\mathrm{n0}^2} + 1} + \frac{1}{2}} \approx -1 - \frac{2\pi^2\tan\left(\frac{\pi}{M}\right)^2}{M^2 n_0^2}. \tag{D12}$$

The last line in the above equation is Eq. (25) for the case where $\Omega < -2J$. The derivation for the $\Omega > 2J$ case can be done by choosing $\mathrm{Re}(s) < 0$ and following the same steps above to arrive at

$$\Omega' = \sqrt{\frac{1}{2}\sqrt{\frac{16\pi^2\tan^2\left(\frac{\pi}{M}\right)}{M^2\mathrm{n0}^2} + 1} + \frac{1}{2}} \approx 1 + \frac{2\pi^2\tan\left(\frac{\pi}{M}\right)^2}{M^2 n_0^2}, \tag{D13}$$

where the last line in the above equation is Eq. (25) for the case where $\Omega > 2J$. To derive Eq. (26), the method is to use Eq. (12) together with Eq. (16) and Eq. (8). We will also use Eq. (25) derived above, and also Eq. (20) for ρ_0/J. Thereafter, doing an asymptotic expansion about $\frac{1}{n_0} \to 0$ and keeping the lowest order, we obtain Eq. (26).

4. Derivation of Eq. (28)

Firstly, we write our BICs $|\pm\rangle$ as

$$\begin{aligned}|\pm\rangle &= \phi_a^{(\pm)}|1_a\rangle + \int_{-\pi}^{\pi} dk\, e(k)^{\pm}|1_k\rangle \\ &= \phi_a^{(\pm)}|1_a\rangle + \phi_a^{(\pm)}\int_{-\pi}^{\pi} dk\, \frac{G^*(k)}{\Omega_\pm - 2J\cos(k)}|1_k\rangle,\end{aligned} \tag{D14}$$

where $\phi_a^{(\pm)} = \langle 1_a|\pm\rangle$ and $e(k)^{\pm} = \langle 1_k|\pm\rangle$, and $\Omega_\pm$ is the energy of the $|\pm\rangle$ state, respectively. In going from the first line to the second line, we used Eq. (B3). In the second line above, we see that we can clearly factor out a global phase corresponding to

the phase of $\langle 1_a|\pm\rangle$. Hence, without loss of generality, we can write $\phi_a \equiv \phi_a^{(\pm)} = \langle 1_a|\pm\rangle$. Then, we have

$$\begin{aligned}
|\pm\rangle &= \phi_a|1_a\rangle + \phi_a \int_{-\pi}^{\pi} dk\, \frac{G^*(k)}{\Omega_\pm - 2J\cos(k)}|1_k\rangle \\
&= \phi_a|1_a\rangle + \phi_a \int_{-\pi}^{\pi} dk\, \frac{G^*(k)}{\Omega_\pm - 2J\cos(k)} c(k)^\dagger|0\rangle \\
&= \phi_a|1_a\rangle + \phi_a \int_{-\pi}^{\pi} dk\, \frac{G^*(k)}{\Omega_\pm - 2J\cos(k)} \sum_n e^{ikn}\frac{1}{\sqrt{2\pi}} b_n^\dagger|0\rangle \\
&= \phi_a|1_a\rangle + \phi_a \int_{-\pi}^{\pi} dk\, \frac{(\rho_0/2\sqrt{\pi})\sum_{l=0}^{M-1} e^{-ikn_l}}{\Omega_\pm - 2J\cos(k)} \sum_n e^{ikn}\frac{1}{\sqrt{2\pi}} b_n^\dagger|0\rangle \\
&= \phi_a|1_a\rangle + \sum_n \underbrace{\frac{\rho_0\phi_a}{2\pi}\sum_{l=0}^{M-1}\int_{-\pi}^{\pi} dk\, \frac{e^{ik(n-n_l)}}{\Omega_\pm - 2J\cos(k)}}_{\equiv\phi_{n,\pm}} b_n^\dagger|0\rangle, \qquad \text{(D15)}
\end{aligned}$$

Thereafter, to evaluate $\phi_{n,\pm}$, we note that

$$\begin{aligned}
\phi_{n,\pm} &= \frac{\rho_0\phi_a}{2\pi}\sum_{l=0}^{M-1}\int_{-\pi}^{\pi} dk\, \frac{e^{ik(n-n_l)}}{\Omega_\pm - 2J\cos(k)} \\
&= \frac{\rho_0\phi_a}{2\pi}\sum_{l=0}^{M-1} I_{n-n_l}(s = -i\Omega_\pm + 0^+), \qquad \text{(D16)}
\end{aligned}$$

where $I_{n-n_l}(s)$ is given by Eq. (D1).

APPENDIX E: PROOF THAT THERE IS NO OSCILLATING BIC WITH $M = 2$

For $n = 2$, we have

$$|G(k)|^2 = \frac{\rho_0^2}{\pi}[1 + \cos(kn_0)], \qquad \text{(E1)}$$

which gives us

$$\Sigma(s) = \frac{-2i\rho_0^2}{\sqrt{s^2 + 4J}}\left[1 + \left(\frac{-i\sqrt{s^2 + 4J^2} + is}{2J}\right)^{n_0}\right]. \qquad \text{(E2)}$$

Thus, we have

$$\begin{aligned}
\Sigma(s = -i\Omega) &= \frac{-2i\rho_0^2}{\sqrt{4J - \Omega^2}}\left[1 + \left(\frac{-i\sqrt{4J^2 - \Omega^2} + \Omega}{2J}\right)^{n_0}\right] \\
&= \frac{-2i\rho_0^2}{\sqrt{4J - \Omega^2}}[1 + \cos(n_0\theta) + i\sin(n_0\theta)], \qquad \text{(E3)}
\end{aligned}$$

where $\theta = \arctan(\frac{-\sqrt{4J^2-\Omega^2}}{\Omega})$ and $-2J < \Omega < 2J$. Using $\Delta(\Omega) = \mathrm{Re}[\Sigma(s = -i\Omega + 0^+)]$, we have

$$\Omega - \omega_a = \frac{2\rho_0^2}{\sqrt{4J - \Omega^2}}\sin(n_0\theta). \qquad \text{(E4)}$$

Furthermore, enforcing $|G(k)|^2 = 0$ gives us

$$k = (2l + 1)\frac{\pi}{n_0}, \qquad \text{(E5)}$$

where l is an integer. Hence, we have

$$\Omega = 2J\cos\left[\frac{\pi}{n_0}(2l + 1)\right], \qquad \text{(E6)}$$

which we can substitute into $\theta = \arctan(\frac{-\sqrt{4J^2-\Omega^2}}{\Omega})$ to get

$$\theta = -\frac{\pi}{n_0}(2l + 1). \qquad \text{(E7)}$$

Substituting the above expression into Eq. (E4), we have

$$\Omega = \omega_a. \qquad \text{(E8)}$$

Hence, when we have $K = 2$ legs in our giant atom, there is only one BIC at the frequency $\Omega = \omega_a$, provided that

$$\omega_a = \Omega = 2J\cos\left[\frac{\pi}{n_0}(2l + 1)\right]. \qquad \text{(E9)}$$

Otherwise, there is no BIC for $K = 2$ legs. Moreover, since we only have one BIC, it is impossible to get an oscillating BIC, which requires at least two BICs at two different frequencies in the band.

APPENDIX F: COMPARISON OF THE OSCILLATING BIC CONDITIONS WITH CONTINUOUS WAVEGUIDE

For M coupling points, and setting $\omega_a = 0$, the oscillating BIC found for a continuous (linearized) waveguide in Ref. [26] is formed from the superposition of two BICs with energies

$$\Omega_c = \pm\frac{1}{2}M\gamma\cot\left(\frac{n\pi}{M}\right), \quad n = 1, 2, \ldots, \lfloor M/2\rfloor, \qquad \text{(F1)}$$

where γ is the giant atom decay rate into the waveguide. In our case, γ corresponds to ρ_0^2/J. From Eq. (19) and Eq. (20), we have, for our case,

$$\begin{aligned}
\Omega_{\mathrm{BIC}} &= \pm 2J\sin\left(\frac{2\pi}{Mn_0}\right) = \pm 2\gamma\frac{J^2}{\rho_0^2}\sin\left(\frac{2\pi}{Mn_0}\right) \\
&= \pm\frac{1}{2}M\gamma\cot\left(\frac{\pi}{M}\right)\sec\left(\frac{2\pi}{Mn_0}\right), \qquad \text{(F2)}
\end{aligned}$$

which looks similar to the continuous-waveguide result for $n = 1$. In fact, in the regime where (Mn_0) is large such that $\sec[2\pi/(Mn_0)] \approx 1$, the oscillating BIC energies are approximately the same as Ω_c.

[1] A. D. Ludlow, M. M. Boyd, J. Ye, E. Peik, and P. O. Schmidt, Optical atomic clocks, Rev. Mod. Phys. **87**, 637 (2015).

[2] C. D. Bruzewicz, J. Chiaverini, R. McConnell, and J. M. Sage, Trapped-ion quantum computing: Progress and challenges, Appl. Phys. Rev. **6**, 021314 (2019).

[3] L.-M. Duan and C. Monroe, Colloquium: Quantum networks with trapped ions, Rev. Mod. Phys. **82**, 1209 (2010).

[4] C. Monroe, W. C. Campbell, L.-M. Duan, Z.-X. Gong, A. V. Gorshkov, P. W. Hess, R. Islam, K. Kim, N. M. Linke, G. Pagano, P. Richerme, C. Senko, and N. Y. Yao, Programmable quantum simulations of spin systems with trapped ions, Rev. Mod. Phys. **93**, 025001 (2021).

[5] C. Cohen-Tannoudji, J. Dupont-Roe, and G. Grynberg, *Atom-Photon Interactions Basic Processes and Applications* (John Wiley & Sons, 1998).

[6] Z. Liao, X. Zeng, H. Nha, and M. S. Zubairy, Photon transport in a one-dimensional nanophotonic waveguide QED system, Phys. Scr. **91**, 063004 (2016).

[7] D. Roy, C. M. Wilson, and O. Firstenberg, Colloquium: Strongly interacting photons in one-dimensional continuum, Rev. Mod. Phys. **89**, 021001 (2017).

[8] J.-T. Shen and S. Fan, Coherent Single Photon Transport in a One-Dimensional Waveguide Coupled with Superconducting Quantum Bits, Phys. Rev. Lett. **95**, 213001 (2005).

[9] J. T. Shen and S. Fan, Coherent photon transport from spontaneous emission in one-dimensional waveguides, Opt. Lett. **30**, 2001 (2005).

[10] M. Bajcsy, S. Hofferberth, V. Balic, T. Peyronel, M. Hafezi, A. S. Zibrov, V. Vuletic, and M. D. Lukin, Efficient All-Optical Switching Using Slow Light within a Hollow Fiber, Phys. Rev. Lett. **102**, 203902 (2009).

[11] A. Akimov, A. Mukherjee, C. Yu, D. Chang, A. Zibrov, P. Hemmer, H. Park, and M. Lukin, Generation of single optical plasmons in metallic nanowires coupled to quantum dots, Nature (London) **450**, 402 (2007).

[12] A. Huck and U. L. Andersen, Coupling single emitters to quantum plasmonic circuits, Nanophotonics **5**, 483 (2016).

[13] M. Arcari, I. Söllner, A. Javadi, S. Lindskov Hansen, S. Mahmoodian, J. Liu, H. Thyrrestrup, E. H. Lee, J. D. Song, S. Stobbe, and P. Lodahl, Near-Unity Coupling Efficiency of a Quantum Emitter to a Photonic Crystal Waveguide, Phys. Rev. Lett. **113**, 093603 (2014).

[14] O. Astafiev, A. M. Zagoskin, A. A. Abdumalikov, Jr., Yu. A. Pashkin, T. Yamamoto, K. Inomata, Y. Nakamura, and J. S. Tsai, Resonance fluorescence of a single artificial atom, Science **327**, 840 (2010).

[15] O. V. Astafiev, A. A. Abdumalikov, A. M. Zagoskin, Yu. A. Pashkin, Y. Nakamura, and J. S. Tsai, Ultimate On-Chip Quantum Amplifier, Phys. Rev. Lett. **104**, 183603 (2010).

[16] A. A. Abdumalikov, O. Astafiev, A. M. Zagoskin, Yu. A. Pashkin, Y. Nakamura, and J. S. Tsai, Electromagnetically Induced Transparency on a Single Artificial Atom, Phys. Rev. Lett. **104**, 193601 (2010).

[17] D. E. Chang, J. S. Douglas, A. González-Tudela, C.-L. Hung, and H. J. Kimble, Colloquium: Quantum matter built from nanoscopic lattices of atoms and photons, Rev. Mod. Phys. **90**, 031002 (2018).

[18] X. Gu, A. F. Kockum, A. Miranowicz, Y.-xi Liu, and F. Nori, Microwave photonics with superconducting quantum circuits, Phys. Rep. **718–719**, 1 (2017).

[19] A. S. Sheremet, M. I. Petrov, I. V. Iorsh, A. V. Poshakinskiy, and A. N. Poddubny, Waveguide quantum electrodynamics: Collective radiance and photon-photon correlations, arxiv.2103.06824.

[20] A. Frisk Kockum, P. Delsing, and G. Johansson, Designing frequency-dependent relaxation rates and Lamb shifts for a giant artificial atom, Phys. Rev. A **90**, 013837 (2014).

[21] A. Frisk Kockum, Quantum optics with giant atoms-The first five years, in *International Symposium on Mathematics, Quantum Theory, and Cryptography*, edited by T. Takagi, M. Wakayama, K. Tanaka, N. Kunihiro, K. Kimoto, and Y. Ikematsu (Springer Singapore, Singapore, 2021) pp. 125–146.

[22] A. F. Kockum, G. Johansson, and F. Nori, Decoherence-Free Interaction between Giant Atoms in Waveguide Quantum Electrodynamics, Phys. Rev. Lett. **120**, 140404 (2018).

[23] B. Kannan, M. Ruckriegel, D. Campbell, A. Frisk Kockum, J. Braumüller, D. Kim, M. Kjaergaard, P. Krantz, A. Melville, B. Niedzielski, A. Vepsäläinen, R. Winik, J. Yoder, F. Nori, T. Orlando, S. Gustavsson, and W. Oliver, Waveguide quantum electrodynamics with superconducting artificial giant atoms, Nature (London) **583**, 775 (2020).

[24] L. Guo, A. Grimsmo, A. F. Kockum, M. Pletyukhov, and G. Johansson, Giant acoustic atom: A single quantum system with a deterministic time delay, Phys. Rev. A **95**, 053821 (2017).

[25] G. Andersson, B. Suri, L. Guo, T. Aref, and P. Delsing, Non-exponential decay of a giant artificial atom, Nat. Phys. **15**, 1123 (2019).

[26] L. Guo, A. F. Kockum, F. Marquardt, and G. Johansson, Oscillating bound states for a giant atom, Phys. Rev. Res. **2**, 043014 (2020).

[27] A. L. Jones, Coupling of optical fibers and scattering in fibers, J. Opt. Soc. Am. **55**, 261 (1965).

[28] S. Somekh, E. Garmire, A. Yariv, H. L. Garvin, and R. G. Hunsperger, Channel optical waveguide directional couplers, Appl. Phys. Lett. **22**, 46 (1973).

[29] S. Longhi, Photonic simulation of giant atom decay, Opt. Lett. **45**, 3017 (2020).

[30] S. Longhi, Rabi oscillations of bound states in the continuum, Opt. Lett. **46**, 2091 (2021).

[31] T. Ramos, B. Vermersch, P. Hauke, H. Pichler, and P. Zoller, Non-Markovian dynamics in chiral quantum networks with spins and photons, Phys. Rev. A **93**, 062104 (2016).

[32] F. H. Stillinger and D. R. Herrick, Bound states in the continuum, Phys. Rev. A **11**, 446 (1975).

[33] Y. Plotnik, O. Peleg, F. Dreisow, M. Heinrich, S. Nolte, A. Szameit, and M. Segev, Experimental Observation of Optical

Bound States in the Continuum, Phys. Rev. Lett. **107**, 183901 (2011).

[34] C. W. Hsu, B. Zhen, A. D. Stone, J. D. Joannopoulos, and M. Soljačić, Bound states in the continuum, Nat. Rev. Mater. **1**, 16048 (2016).

[35] S. Longhi, Bound states in the continuum in a single-level Fano-Anderson model, Eur. Phys. J. B **57**, 45 (2007).

[36] M. Johnsson and K. Mølmer, Storing quantum information in a solid using dark-state polaritons, Phys. Rev. A **70**, 032320 (2004).

[37] C.-P. Yang, S.-I. Chu, and S. Han, Quantum Information Transfer and Entanglement with SQUID Qubits in Cavity QED: A Dark-State Scheme with Tolerance for Nonuniform Device Parameter, Phys. Rev. Lett. **92**, 117902 (2004).

[38] E. Munro, L. C. Kwek, and D. E. Chang, Optical properties of an atomic ensemble coupled to a band edge of a photonic crystal waveguide, New J. Phys. **19**, 083018 (2017).

[39] M. J. Hartmann, F. G. S. L. Brandao, and M. B. Plenio, Quantum many-body phenomena in coupled cavity arrays, Laser Photonics Rev. **2**, 527 (2008).

[40] A. Majumdar, A. Rundquist, M. Bajcsy, V. D. Dasika, S. R. Bank, and J. Vučković, Design and analysis of photonic crystal coupled cavity arrays for quantum simulation, Phys. Rev. B **86**, 195312 (2012).

[41] D. N. Christodoulides, F. Lederer, and Y. Silberberg, Discretizing light behaviour in linear and nonlinear waveguide lattices, Nature (London) **424**, 817 (2003).

[42] S. Longhi, Quantum-optical analogies using photonic structures, Laser Photonics Rev. **3**, 243 (2009).

[43] A. Szameit and S. Nolte, Discrete optics in femtosecond-laser-written photonic structures, J. Phys. B: At. Mol. Opt. Phys. **43**, 163001 (2010).

[44] A. Aspuru-Guzik and P. Walther, Photonic quantum simulators, Nat. Phys. **8**, 285 (2012).

[45] I. L. Garanovich, S. Longhi, A. A. Sukhorukov, and Y. S. Kivshar, Light propagation and localization in modulated photonic lattices and waveguides, Phys. Rep. **518**, 1 (2012).

[46] Z.-Q. Jiao, J. Gao, W.-H. Zhou, X.-W. Wang, R.-J. Ren, X.-Y. Xu, L.-F. Qiao, Y. Wang, and X.-M. Jin, Two-dimensional quantum walks of correlated photons, Optica **8**, 1129 (2021).

[47] T. B. H. Tentrup, T. Hummel, T. A. W. Wolterink, R. Uppu, A. P. Mosk, and P. W. H. Pinkse, Transmitting more than 10 bit with a single photon, Opt. Express **25**, 2826 (2017).

[48] H. Tang, L. Banchi, T.-Y. Wang, X.-W. Shang, X. Tan, W.-H. Zhou, Z. Feng, A. Pal, H. Li, C.-Q. Hu, M. S. Kim, and X.-M. Jin, Generating Haar-Uniform Randomness Using Stochastic Quantum Walks on a Photonic Chip, Phys. Rev. Lett. **128**, 050503 (2022).

[49] G. Crowder, H. Carmichael, and S. Hughes, Quantum trajectory theory of few-photon cavity-qed systems with a time-delayed coherent feedback, Phys. Rev. A **101**, 023807 (2020).

[50] S. Arranz Regidor and S. Hughes, Cavitylike strong coupling in macroscopic waveguide QED using three coupled qubits in the deep non-Markovian regime, Phys. Rev. A **104**, L031701 (2021).

[51] P.-O. Guimond, A. Roulet, H. N. Le, and V. Scarani, Rabi oscillation in a quantum cavity: Markovian and non-Markovian dynamics, Phys. Rev. A **93**, 023808 (2016).

[52] O. Černotík, A. Dantan, and C. Genes, Cavity Quantum Electrodynamics with Frequency-Dependent Reflectors, Phys. Rev. Lett. **122**, 243601 (2019).

[53] L. Du, M.-R. Cai, J.-H. Wu, Z. Wang, and Y. Li, Single-photon nonreciprocal excitation transfer with non-Markovian retarded effects, Phys. Rev. A **103**, 053701 (2021).

[54] A. González-Tudela, C. S. Muñoz, and J. I. Cirac, Engineering and Harnessing Giant Atoms in High-Dimensional Baths: A Proposal for Implementation with Cold Atoms, Phys. Rev. Lett. **122**, 203603 (2019).

[55] L. Du, Y. Zhang, J.-H. Wu, A. F. Kockum, and Y. Li, Giant Atoms in a Synthetic Frequency Dimension, Phys. Rev. Lett. **128**, 223602 (2022).

[56] H. Xiao, L. Wang, Z.-H. Li, X. Chen, and L. Yuan, Bound state in a giant atom-modulated resonators system, npj Quantum Inf. **8**, 80 (2022).